Hertzian impact: Experimental study of the force pulse and resulting stress waves

Gregory C. McLaskey[a)] and Steven D. Glaser
Department of Civil and Environmental Engineering, University of California, Berkeley, 621A Sutardja Dai Hall (CITRIS Building), Berkeley, California 94720-1758

(Received 22 March 2010; revised 11 June 2010; accepted 21 June 2010)

Ball impact has long been used as a repeatable source of stress waves in solids. The amplitude and frequency content of the waves are a function of the force-time history, or force pulse, that the ball imposes on the massive body. In this study, Glaser-type conical piezoelectric sensors are used to measure vibrations induced by a ball colliding with a massive plate. These measurements are compared with theoretical estimates derived from a marriage of Hertz theory and elastic wave propagation. The match between experiment and theory is so close that it not only facilitates the absolute calibration the sensors but it also allows the limits of Hertz theory to be probed. Glass, ruby and hardened steel balls 0.4 to 2.5 mm in diameter were dropped onto steel, glass, aluminum, and polymethylmethacrylate plates at a wide range of approach velocities, delivering frequencies up to 1.5 MHz into these materials. Effects of surface properties and yielding of the plate material were analyzed via the resulting stress waves and simultaneous measurements of the ball's coefficient of restitution. The sensors are sensitive to surface normal displacements down to about ±1 pm in the frequency range of 20 kHz to over 1 MHz.
 [DOI: 10.1121/1.3466847]

PACS number(s): 43.40.Kd, 43.38.Fx, 43.64.Yp [RLW] Pages: 1087–1096

I. INTRODUCTION

The normal impact of a ball on a massive body has been extensively used as a source of stress waves for non-destructive testing techniques such as impact echo and acoustic emission (e.g., Sansalone and Street, 1997; Breckenridge *et al.*, 1990; Lange and Ustinov, 1983). Ball impact is in some cases preferable to sources such as pencil lead fracture (Hsu, 1977) or pulsed laser (Scruby and Drain, 1990) because the stress wave signature that it imparts is intimately related to the force pulse that ball imposes on the massive body, which can be calculated from Hertzian contact theory (Hunter, 1957; Reed, 1985). Hertz (1882) contact model is both elastic and quasistatic in nature; it neglects to consider both radiated elastic waves and anelastic effects, such as plasticity and viscoelasticity. Hertz law has been used beyond the limits of its validity on the basis that it accurately predicts those impact parameters which can be experimentally verified (Love, 1927). As test methods become more precise, and theoretical and numerical studies more detailed, there is a need to experimentally validate the Hertzian impact model and to quantitatively evaluate its limits.

This paper presents a systematic study of ball impact as a source of stress waves for a number of different material combinations. Impact-generated vibrations were recorded with an array of pm sensitive high-fidelity sensors, and by carefully eliminating the wave propagation effects, estimates of the force pulse were obtained and compared to the Herztian-derived pulse. We experimentally verify the Reed (1985) correction to Hunter's (1957) calculation of the force pulse by measuring the locations of zeros in the spectral content of measured waves. The validity of Hertzian theory is also assessed for cases in which plastic deformation and surface effects absorb some of the ball's kinetic energy during the collision. Our methodology is similar to that of previous researchers (Crook, 1952; Goldsmith and Lyman, 1960; Chang and Sun, 1989; Buttle and Scruby, 1990) but employs a more exact treatment of wave propagation effects, and takes into careful consideration the response function of the sensors used to record the stress waves. The conical piezoelectric sensors used in this work were developed in our laboratory and were absolutely calibrated by comparing results from capillary fracture and ball impact calibration sources.

The present work focuses on the measurement of two impact parameters: the force time history, or force pulse, that the ball imposes on the massive body, and the coefficient of restitution (e)—defined as the ratio of the magnitudes of the rebound and approach velocities of the ball. The force pulse describes the ball's change in momentum over time, shown to be intimately related to the stress waves radiated from the collision, while e is a measure of the total kinetic energy lost to non-conservative processes such as radiated stress waves, plastic deformation, and viscoelasticity (Falcon *et al.*, 1998). We examine the applicability of different Hertzian derivations of the force pulse published by Hunter (1957) and Reed (1985).

II. METHODS

A schematic of the test setup is shown in Fig. 1. As depicted, the collision of a ball (a) at location (b) on a mas-

[a)]Author to whom correspondence should be addressed. Electronic mail: gmclaskey@berkeley.edu

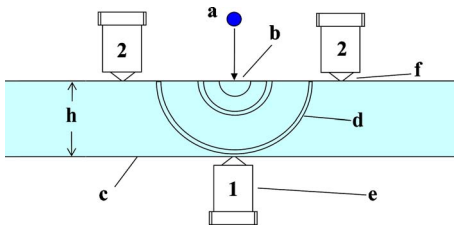

FIG. 1. (Color online) Schematic diagram of the test setup which includes a massive plate, (a), and a ball, (b), colliding at the source location, (c), which generates radiated stress waves, (d), detected by an array of sensors, (e), each of which employs a conical piezoelectric sensing element, (f).

sive plate (c) of thickness h is the source of the radiating stress waves (d) which are detected by an array of sensors (e). The signals recorded and analyzed are a function of the source, the test block and array geometry, and the sensors themselves. Under the Green's function formalism used in this study, the source (either ball impact or glass capillary fracture) is represented by a force function, the propagation effects are represented by the Green's function for a particular plate material and source-sensor orientation, and the effects of the sensor are represented by the sensor's instrument response function.

A. Test plates and Green's functions

For these experiments, test blocks consisted of plates of homogeneous materials. Material properties, geometry, and P-wave travel times of the four plates used in this study are shown in Table I. The propagation of elastic waves in these materials is assumed to be well modeled by the elastodynamic equations of motion for an elastic continuum (Graff, 1975, Eq. 5.1.2; Aki and Richards, 1980, Eq. 4.1). Solutions to these equations can be found in the form of a Green's function, $G_{in}(x,t;\xi,\tau)$, which describes the displacement in the i direction at point x at time t due to a unit impulsive force at location ξ in the direction n at time τ (Aki and Richards, 1980, Eq. 2.36). If the location ξ at which the dynamic force field acts is replaced by a point ξ_0, the Green's function can be expanded in a Taylor series about this point (Stump and Johnson, 1977). By taking only the first term of this series, the displacement at the sensor location can be expressed as

$$u_i(x,t) = G_{in}(x,t;\xi_0,\tau) \otimes f_n(\xi_0,\tau), \tag{1}$$

where $\otimes$ represents convolution in time and $f_n(\xi_0,\tau)$ is the source function which is the sum of all forces in ξ. If displacements $u_i(t)$ and forces $f_n(\tau)$ are assumed to act only in the plate-normal direction, Eq. (1) reduces to the scalar equation:

$$u_3(t) = g_{33}(x_0,t;\xi_0,\tau) \otimes f_3(\xi_0,\tau), \tag{2}$$

where the coordinate system is chosen so that "3" denotes the plate normal direction. Little error is expected to be introduced by these assumptions because sources such as a ball impact or a glass capillary fracture produce forces that act on regions which are small compared to measured wavelengths, and the direction of imposed forces is very nearly normal to the plane of the plate. Likewise, the sensors used in this study are sensitive only to displacements normal to the surface of the plate and the sensor contact area is typically quite small compared to measured wavelengths.

For times less than t_{max} (see Table I), the plate can be considered infinite; therefore Green's functions were calculated using a generalized ray theory code for infinite plates (Hsu, 1985, similar to Ceranoglu and Pao, 1981). This solution was checked by the theoretical calculations of Knopoff (1958) at the epicentral location, and Pekeris (1955) on the same surface for times preceding the arrival of the first P wave reflection, and by finite element models (McLaskey and Glaser, 2009).

The sensor array, shown in Fig. 1, is configured such that one sensor is located directly opposite and on the underside of the source location (Position 1), and two more are located 45 mm from the source on the loaded surface of the plate (Position 2). The Green's functions for sensor Positions 1 and 2 on the steel plate, shown in Figs. 2(a) and 2(b), respectively, are plotted against $t_n = t/t_w$ where t_w is the P-wave travel time through the plate thickness. The corresponding power spectra are shown in Fig. 2(c). The spikes at $t_n = 1,3,5$, etc. in Fig. 2(a) correspond to the multiple reflections of the P-wave through the thickness of the plate.

The plates in this study are considered "thick" because, for nearly all collisions considered, the contact duration t_c is less than twice t_w. Therefore, from the ball's perspective, the plate is infinitely thick and plate effects such as those studied by Zener (1941) and the effects of the plate supports could be neglected.

Damping (internal friction or intrinsic attenuation) in each of the plate materials were estimated following the methods of To and Glaser (2005). It was found that, for the frequency range under consideration, only the polymethylmethacrylate (PMMA) plate produced non-negligible damping (Q=80). This damping term was included in PMMA Green's function calculations.

TABLE I. Plate properties: density (ρ), P-wave velocity (c_p), S-wave velocity (c_s), plate thickness (h), side length (w), time taken for P-waves to traverse the thickness of the plate ($t_w = h/c_p$), and time required for P waves to reflect off the plate edge and return to the center ($t_{max} = w/c_p$).

Material	ρ (kg m^{-3})	c_p (mm μs^{-1})	c_s (mm μs^{-1})	h (mm)	w (mm)	t_w (μs)	t_{max} (μs)
Steel	7850	5.90	3.23	50.1	610	8.49	100
Aluminum	2700	6.35	3.17	32.4	610	5.09	96
Glass	2480	5.90	3.50	24.4	760	4.14	125
PMMA	1190	2.81	1.40	50.1	940	17.83	220

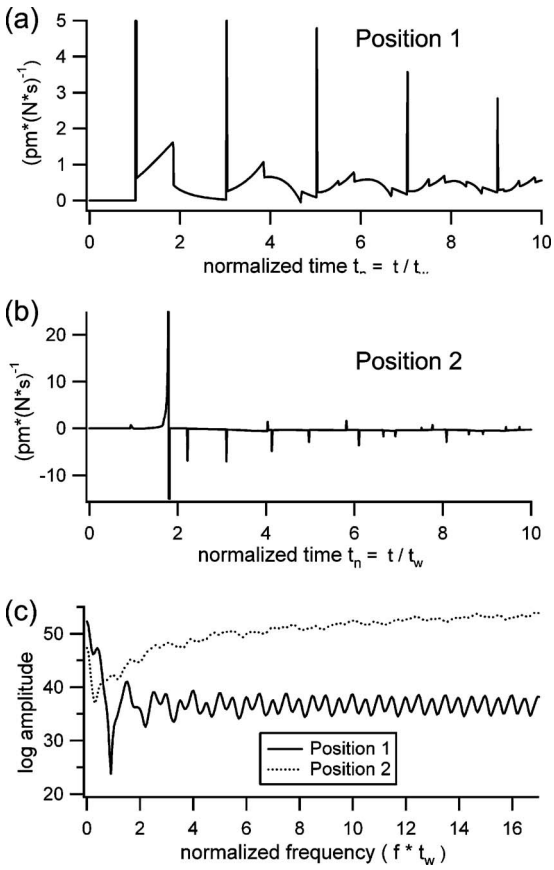

FIG. 2. Green's functions for sensor Position 1, (a), and sensor Position 2, (b), and their corresponding amplitude spectra, (c).

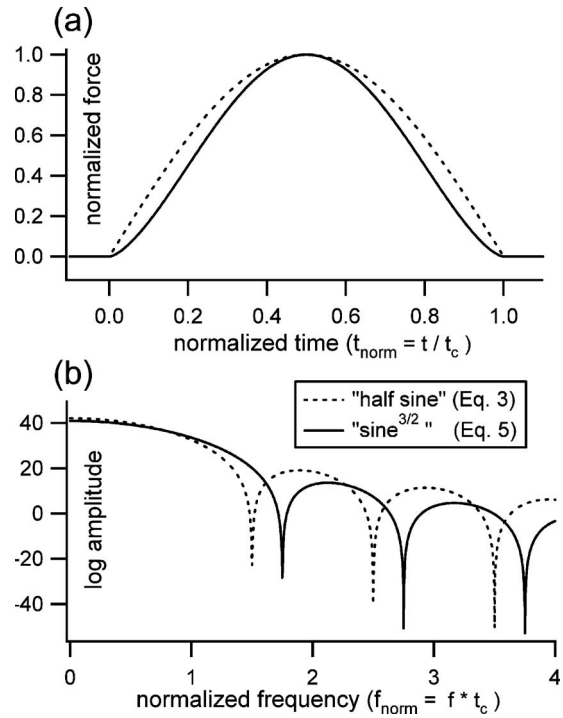

FIG. 3. Two different force pulses (a) and their spectral content (b), both derived from Hertzian contact laws. The locations of zeros in the spectral content are used for quantitative evaluation.

B. The source function and Hertzian impact

While a number of different seismic sources have been explored for calibration purposes (Breckenridge *et al.*, 1990), two dissimilar sources were chosen for this work: glass capillary fracture and ball impact. The sudden fracture of a small length (2 mm) of 0.25 mm diameter thin-walled glass capillary laid horizontally and slowly loaded normal to the plate is known to present a force function into the test block which is very nearly equal to a step function with a rise time of less than 200 ns (Breckenridge *et al.*, 1975). The amplitude of the step is equal to the force at which the fracture occurs (usually between about 2 and 20 N), which can be independently measured for absolute calibration. A small amount of variability (approximately 4 dB/MHz from 0.5–1.5 MHz) was measured in the shape of the frequency spectra of this source, likely due to variability in the wall thickness and fracture strength of the glass.

A complete derivation of Hertzian impact theory can be found in Goldsmith (2001), Johnson (1985), and Love (1927); we present only an abbreviated formulation of the equations useful for this study. The impulsive force (force pulse) that a ball imparts to a massive body was derived by Hunter (1957) and is very well approximated by a "half sine" pulse of the form

$$f_H(t) = f_{H\,\max} \sin(\pi t/t_c), \quad 0 \le |t| \le t_c,$$

$$f_H(t) = 0 \quad \text{otherwise}, \tag{3}$$

where the contact time

$$t_c = 4.53(4\rho_1 \pi(\delta_1 + \delta_2)/3)^{2/5} R_1 v_0^{-1/5}. \tag{4}$$

For Eqs. (3) and (4), $\delta_i = (1-\nu_i^2)/(\pi E_i)$, and E, and ν are the Young's modulus and Poisson's ratio, respectively. Subscript 1 refers to the material of the ball and subscript 2 refers to the material of the plate. The constant $f_{H\,\max}$ depends on the material properties of the ball and massive body as well as R_1, v_0, and ρ_1, which are the radius, approach velocity, and density of the ball, respectively. Time t=0 is the initiation of contact.

Alternatively, Reed (1985), made a correction to Hunter's calculation by using the force deformation relation $f = k_1 \alpha^{3/2}$ instead of Newton's second law. (The constant k_1 depends on the geometry and material properties of the two bodies.) The result is a formulation:

$$f(t) = f_{\max} \sin(\pi t/t_c)^{3/2}, \quad 0 \le |t| \le t_c$$

$$f(t) = 0 \quad \text{otherwise} \tag{5}$$

where the maximum force is

$$f_{\max} = 1.917 \rho_1^{3/5} (\delta_1 + \delta_2)^{-2/5} R_1^2 v_0^{6/5}. \tag{6}$$

This force pulse is inserted into Eq. (2) to produce theoretical estimates of displacements, and it is central to estimates of the amount of energy contained in radiated stress waves (Hunter, 1957; Hutchings, 1979; Reed, 1985).

The two variations of the Hertz-derived force pulse are shown in Fig. 3: the "half sine" pulse used by Hunter [Eq. (3)], and the "$\sin^{3/2}$" pulse used by Reed [Eq. (5)] (all nor-

malized in amplitude). The magnitudes of the Fourier transforms of these pulses are plotted in Fig. 3(b) as a function of normalized frequency. The shape of the spectral content of this source consists of a series of lobes separated by zeros, or frequencies void of spectral amplitude. The zero frequency which separates the main lobe from n^{th} side lobe can be expressed as $f_{zero,n}=A_n/t_c$ where A_n is a dimensionless number which depends on the shape of the pulse. $A_n=n+0.5$ for the "half sine" pulse, and $A_n=n+0.75$ for the "$\sin^{3/2}$" pulse.

C. Sensors and the instrument response function

Piezoelectric sensors were used because of their superior sensitivity compared to capacitive transducers (Breckenridge and Greenspan, 1981) and optical methods (Boltz and Fortunko, 1995) and because of the relative ease with which they can be mounted to a specimen in the form of a sensor array. While most piezoelectric transducers take advantage of some mechanical resonance to gain high sensitivity at the expense of loss of bandwidth and signal distortion, the sensors used in this study, which are manufactured in our laboratory, are based on a design developed in the late 1970s intended to provide a more faithful transduction of surface displacement (Proctor, 1982; Greenspan, 1987).

The sensors contain an EBL# 2 PZT-5a (lead-zirconium-titanate composition) truncated cone sensing element. The one part of the sensor in contact with the specimen is the 1.75 mm diameter truncated tip of the conical PZT element which is covered by a thin brass shim (which completes the electrical circuit, and enhances the mechanical bond with the specimen). The sensor is pressed onto the surface of the specimen with a mounting force of about 10 N. Sensitivity greater than many resonant sensors is made possible by the incorporation of an impedance matching JFET driver circuit located adjacent to the base of the PZT cone. This avoids signal loss due to parasitic capacitance. More details on the sensor design are described in Glaser *et al.* (1998).

Conical piezoelectric sensors are reported to have an extremely flat response between 100 kHz and 1 MHz (e.g., Scruby *et al.*, 1986; Proctor, 1982), but because these are contact sensors, the actual response is a function of the impedance match between the sensor and specimen (Breckenridge *et al.*, 1975), causing difficulties in the sensor's absolute calibration. Until now, a calibration on a number of different materials which adequately addresses both amplitude and phase information has been only briefly studied (Miller and McIntire, 1987).

The calibrations performed for this study follow a transfer function approach fully described in Hsu and Breckenridge (1981). In this method, the sensor output v(t) is expressed as the linear convolution of the surface displacement and the sensor's instrument response function:

$$v(t) = u_3(t) \otimes i(t), \tag{7}$$

where $u_3(t)$ is the displacement normal to the surface of the specimen at the sensor location x which would exist in the absence of the sensor [estimated from Eq. (2)]. The complex transfer function of the transducer $I(\omega)=V(\omega)U_3(\omega)^{-1}$ can be found from inversion of the Fourier transform of Eq. (7). The sensor response $I(\omega)=\beta\cdot I_{norm}(\omega)$, where $I_{norm}(\omega)$ is the shape of the frequency response, and β is the absolute sensitivity given a specific $I_{norm}(\omega)$.

Once the transducer response function and Green's function of the plate material/source-sensor orientation have been determined, any or both of these effects can be removed from recorded signals through inversion. This inverse problem is solved in the frequency domain by directly dividing Fourier frequencies, or in the time domain using a least-squares deconvolution strategy (Michaels, 1982; Yilmaz, 1987). Both methods were used in this study, and the accuracy of the inversion is discussed in Sec. IV B.

III. EXPERIMENTS

Three collections of experiments were performed on the four plates described in Table I. For all tests, the setup was identical to that shown in Fig. 1, except that the ball source was in some cases replaced by a capillary fracture. The glass and PMMA plates were left in "as received" condition while the steel and aluminum plates were polished to a mirror finish. The output from each sensor was recorded at 10 M samples per second and 14-bit dynamic range. For spectral estimates, recorded signals were windowed with a Blackman-Harris window centered on the first wave arrival and transformed using a fast Fourier transform algorithm. The length of the window varied for different plate materials but was always less than 2^*t_{max}.

For the calibration tests, five capillary fracture tests were performed on each plate specimen and the force at which fracture occurred was independently measured with a force sensor. Five ball-drop tests using small (0.40 mm and 0.50 mm diameter) ruby balls were also performed. To separate sensor response from source-receiver geometry, one of the sensors in Position 2 was switched with the sensor in Position 1, and the sets of five capillary tests and five ball drops were repeated.

In the second collection of experiments, sets of ball-drop tests were performed using hardened steel balls and ruby balls of 1.00 mm and 2.38 mm in diameter and glass balls of 1.00 mm and 2.5 mm in diameter, at three different drop heights: 0.068 m, 0.127 m, and 0.315 m. For each test, a ball was dropped from a platform of known height, allowed to fall through the air, strike the plate, rebound, and then strike the plate again; this procedure was repeated ten times for each of the selected combinations of drop height, ball size, and ball/plate materials. Signals were recorded for 1.6 ms surrounding the first arrival of the elastic waves produced by the initial collision of the ball on the plate, and for 105 ms surrounding the expected time of the second bounce of the ball on the plate. The incoming velocity of the initial collision was calculated from the known height of the ball drop while the rebound velocity of the same collision was calculated from the time between successive bounces (Bernstein, 1977; Falcon *et al.*, 1998).

For the third set of tests, the ball was dropped from a wide range of heights (1 mm to 1 m) and allowed to bounce repeatedly (tens of times in succession). Stress wave information over the entire time period was recorded at a reduced

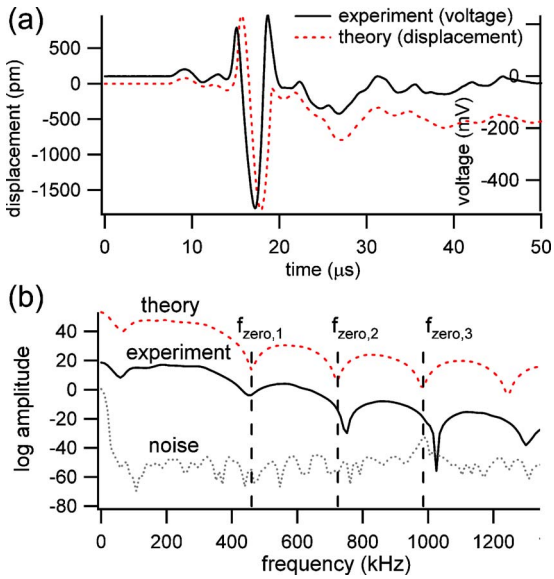

FIG. 4. (Color online) Comparison between theory [using the "$\sin^{3/2}$" Hertzian force pulse, Eq. (5)] and experiment for a 1.00 mm steel ball dropped 315 mm onto a thick aluminum plate. Subtle differences between experiment and theory can be identified by the locations of zeros in the frequency spectra in (b).

sampling rate (500 kHz), and the first wave arrival (determined to ± 2 μs) from each successive impact was used for e calculations (following Bernstein, 1977; and Falcon *et al.*, 1998).

IV. RESULTS

A. F_{zero} results

The frequencies of zeros in the power spectrum of recorded signals ($f_{zero,1}$, $f_{zero,2}$, and $f_{zero,3}$) were estimated from local minima found in the magnitude of the Fourier transform of recorded signals from the sensors in Position 2. An example of one such signal, produced from the collision of a 1.00 mm steel ball dropped 325 mm onto the aluminum plate is plotted in Fig. 4(a) along with the surface normal displacements predicted by theory [Eq. (5) inserted into Eq. (2)]. The transducer sensitivity is approximately 250 mV/nm, and the noise is approximately ± 0.25 mV (± 1 pm). The magnitude of the Fourier transform of the recorded signals and theoretical displacements are plotted in Fig. 4(b) along with the power spectrum of a pure noise signal of the same length.

The results for $f_{zero,1}$, $f_{zero,2}$, and $f_{zero,3}$ for all material combinations are plotted in Fig. 5 on a nondimensionalized frequency scale which is normalized to t_c, found from Eq. (4). The expected f_{zero} locations for the "$\sin^{3/2}$" force pulse are shown as vertical dashed lines for reference. The observed f_{zero} locations strongly favor the "$\sin^{3/2}$" force pulse formulation over the "half sine" pulse described in Sec. II B, thus validating the Reed (1985) correction to Hunter's (1957) theory. This quantitative evaluation of the force pulse does not rely on an accurate calibration of the sensors. Note that the results for ruby and steel balls colliding with the steel and aluminum plates produce slightly low $f_{zero,1}$, and slightly

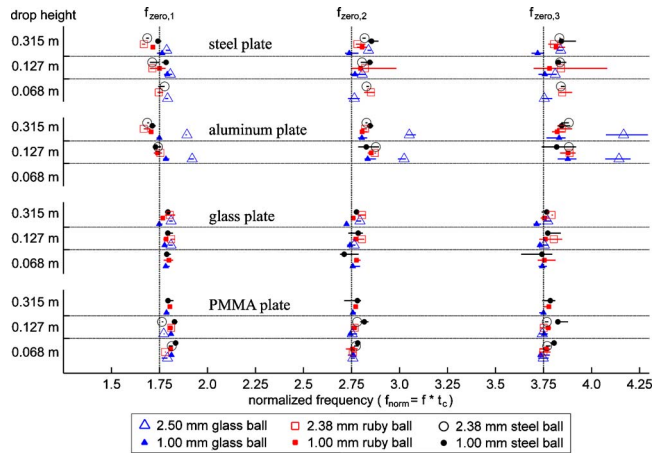

FIG. 5. (Color online) The frequencies of the first three zeros ($f_{zero,1}$, $f_{zero,2}$, and $f_{zero,3}$), found from local minima in the power spectra of recorded signals, are plotted against a nondimensionalized frequency parameter. The vertical grid lines correspond to expected f_{zero} frequencies based on a $\sin^{3/2}$ force pulse formulation derived from Hertz theory [Eq. (5)]. The symbol locations indicate the median frequency for each set of ten ball-drop tests while the horizontal error bar extends from the first to the third quartiles of the set of ten tests.

high $f_{zero,2}$, and $f_{zero,3}$, while the collisions on Glass and PMMA plates are more consistent with theory (these deviations are discussed in Sec. V B).

B. Calibration tests

Estimates of the instrument response function $I(\omega)$ for one sensor, found from the ratio of complex Fourier frequencies obtained from experimental data to those obtained from theory, are shown in Fig. 6 for a variety of different source and plate combinations. The results from the four different

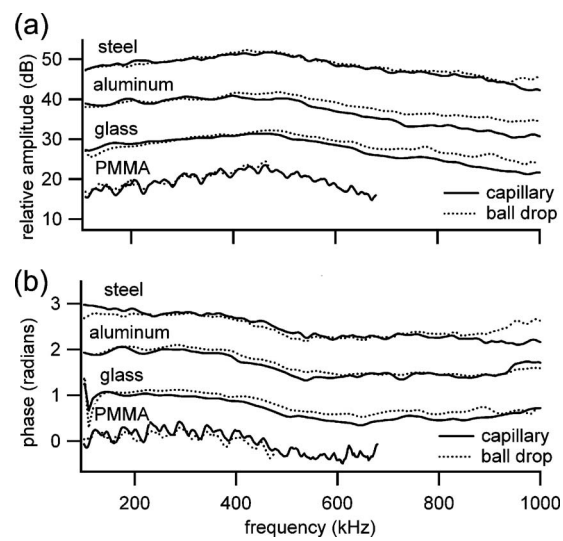

FIG. 6. The amplitude, (a), and phase, (b), estimates of the instrument response function of one of the conical piezoelectric sensors coupled to the four different test plates (each one offset for clarity) over a frequency range of 100 kHz to 1 MHz. Each line is the average of 3–5 calibration tests—either ball drops or capillary fractures (outliers were removed). Note that the roughness in both the amplitude and phase (especially apparent in the PMMA trace) is due to a slight mismatch between the Green's function estimates and the actual impulse responses of the plates.

plate materials are offset for clarity, and are shown only in frequency ranges for which a signal to noise ratio of at least 20 dB was attained.

Some variation was observed in instrument response between different sensors, but in all cases the underlying amplitude and phase spectra of the instrument response were found to be smooth and flat enough to make its removal via deconvolution a relatively straightforward affair. The results presented in Fig. 6 show that the general shape of the instrument response ($I_{norm}(\omega)$) is unchanged (to within ± 3 dB) when coupled to the four different plate materials. The sensor calibration results from Position 1 are shown for PMMA, while the results for Position 2 are shown for the other three materials. The roughness in both the amplitude and phase response (especially apparent in the PMMA trace) is due to a slight mismatch between the Green's function estimates and the actual impulse responses of the plates. Other than increased roughness, calibration results for steel, aluminum, and glass obtained from sensor Position 1 did not differ appreciably (no more than ± 3 dB) from those obtained from Position 2. The level of agreement between ball-source and capillary-source sensor calibrations illustrates that either of these sources can be successfully used for sensor calibration purposes, but the divergence at high frequencies between the ball and capillary test results establishes a bound on the reliability of both the capillary fracture model (step function) and the Hertzian impact model [Eq. (5)].

The absolute sensitivity of the sensor, β, was found to be, on average, about 15 dB less sensitive when coupled to PMMA (45 mV/nm) than when coupled to the steel, aluminum, and glass plates (250 mV/nm). This result is consistent with Miller and McIntire (1987) and is attributed to the lower acoustic impedance of PMMA. On a given material, β varied by as much as a factor of 2 and was affected by the physical bond between the sensor tip and the specimen (affected by couplant, mounting force, and even time of sensor contact). Sensor sensitivity was, on average, 200–250 mV/nm when coupled to Glass, Aluminum, and Steel, and about 45 mV/nm when coupled to PMMA.

The removal of the Green's function by inversion was much more difficult and prone to error than that of the instrument response function because the Green's function is not minimum phase, has an infinite impulse response, and its amplitude and phase spectra are not smooth [as shown in Fig. 2(c)]. Difficulties in this inversion process are well known (e.g., Ching *et al.*, 2004; Michaels *et al.*, 1981), and errors are manifested as "overshoots" and "aftershocks" to the calculated force pulses such as those shown in Fig. 8(b).

C. Impulse and force pulse

The impulse P that the ball imparts to the plate (equal to the ball's change in momentum) is defined as the time integral of the force pulse

$$P = \int f_3(t)dt = m_1|v_f - v_0|, \tag{8}$$

where v_f and m_1 are the rebound velocity and mass of the ball, respectively. The force pulse can be found from the

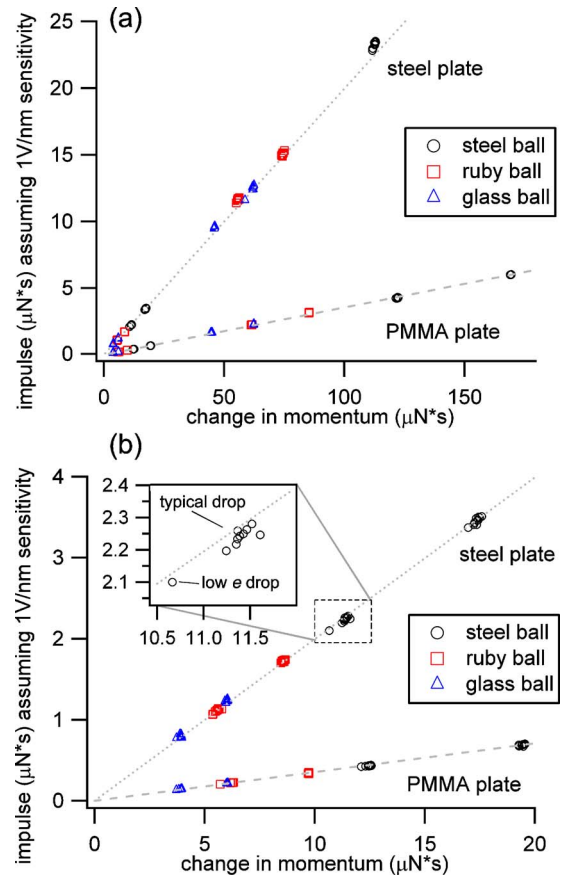

FIG. 7. (Color online) The proportionality between impulse derived from recorded stress waves [Eq. (9)] and the ball's change in momentum is illustrated for 1 to 2.5 mm diameter balls of various materials striking thick steel and PMMA plates (a). The results for the 1 mm diamater balls are shown at greater magnification (b). The results from the ten tests of 1 mm steel balls dropped 127 mm onto the steel plate are shown in more detail in the inset.

inversion of recorded signals, but to circumvent the aforementioned difficulties involved in the removal of the Green's function, the following approximation is made. For force pulses $f_3(t)$ which are of short duration compared to t_w, by integrating Eq. (2) over time, the impulse can be well approximated by

$$\int f_3(t)dt \cong \gamma^{-1} \int_{t_n=0}^{t_n=3} u_3(t)dt, \tag{9}$$

where

$$\gamma = \int_{t_n=0}^{t_n=3} g_{33}(t)dt \tag{10}$$

is a constant which only depends on the Green's function for a given plate material and sensor location and $t_n = t/t_w$. In Eq. (9), displacements $u_3(t)$ are estimated by removing the instrument response $i(t)$ from recorded signals.

In Fig. 7, the impulse that the ball delivers to the plate, calculated from radiated stress wave measurements [Eq. (9)], is graphed against the ball's change in momentum, calculated from v_0 and v_f [Eq. (8)], for balls dropped on steel and PMMA plates. Each group of points corresponds to a set of ten ball drops performed under the same conditions. Figure 7(b) shows the same data at greater magnification. There is a

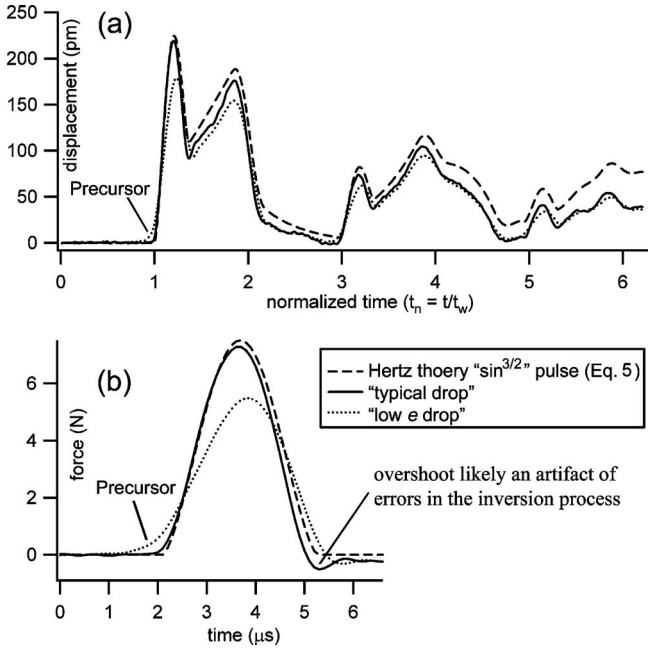

FIG. 8. Normal displacements at sensor Position 1 (directly beneath the location of impact) due to the collision of a 1 mm steel ball dropped 127 mm onto a 50 mm thick steel plate. Small precursory forces which accompany low e collisions can be seen in both the wave amplitudes (a) and the force pulse (b) found from inversion.

linear proportionality between impulse calculated from stress waves and change in momentum observed from incoming and rebound velocities of the ball. The slope of the resulting trend line is equal to the sensor sensitivity β relative to the sensitivity assumed for the impulse calculation (which was 1 V/nm). All of the data lies within ± 0.5 dB of the $\beta = -14$ dB and $\beta = -29$ dB lines shown, even for abnormally low e collisions such as that shown in Fig. 7(b) inset. This comparison serves a means of double checking the absolute sensor sensitivity β over a wide range of amplitudes once the instrument response $I_{norm}(\omega)$ (shown in Fig. 6) has been estimated. Note that the sensor is 15 dB more sensitive when coupled to steel than when coupled to PMMA.

Each set of ball drop tests showed some variability in measured coefficient of restitution, but a few of the collisions showed e markedly lower than the others, with subtle differences in the shape of the force pulse. A well-pronounced example of this aberration is illustrated in Fig. 8 for the case of a 1.00 mm diameter steel ball dropped 127 mm onto the steel plate, but similar results were observed for all types of ball and plate materials tested. Note that the signals shown in Fig. 8 correspond to the same data plotted in Fig. 7(b) inset. In Fig. 8(a), the instrument response function $i(t)$ has been removed from the raw experimental data and resulting displacement time histories are plotted along side synthetic data [obtained by inserting Eq. (5) into Eq. (2)]. The force pulses shown in Fig. 8(b) were found by removing both the instrument response function and the Green's function [shown in Fig. 2(a)] from the recorded signals. Of the data from the ten ball drop tests performed under these conditions, nine of them [the cluster in Fig. 7(b) inset] are very similar to that of the "typical drop" plotted in Fig. 8. The remaining outlier labeled "low e drop" is plotted for comparison. The

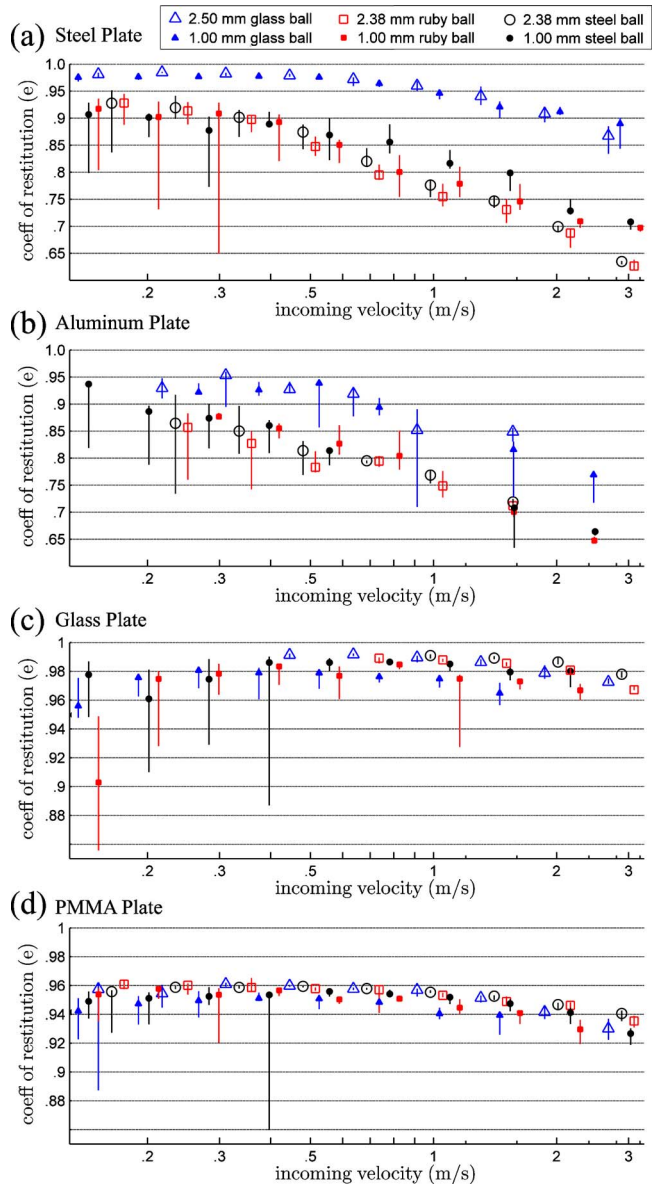

FIG. 9. (Color online) Coefficient of restitution (e) plotted against the log of incoming velocity for all ball and plate material combinations. Data is grouped into logarithmically spaced bins on a velocity scale. Each symbol location denotes the median e from sets of at least four data points, and the vertical error bar extends from the first to the third quartiles. Note that the scale in Figs. 9(a) and 9(b) is different from that in Figs. 9(c) and 9(d).

somewhat-lower-than-average amplitude and small precursory force which precedes the first main wave arrival are typical features of these low-restitution collisions and were observed by every sensor in the array. Low-restitution collisions of this type are thought to be due to surface effects discussed in Sec. V C.

D. Restitution tests

The results of the restitution tests for all plate materials are summarized in Figs. 9 and 10. As previously described, incoming and rebound velocities of the ball were calculated from the time between successive bounces (as in Bernstein, 1977, and Falcon *et al.*, 1998) which was determined from stress wave arrival information and contact times. In the absence of air resistance, the ball's rebound velocity after the

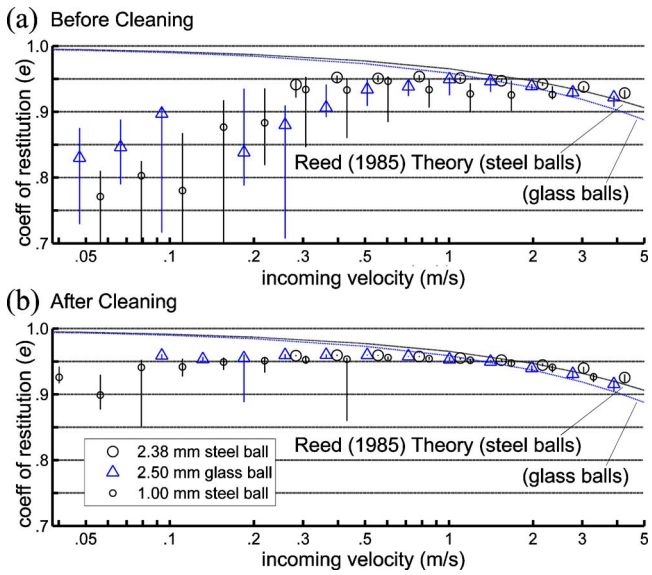

FIG. 10. (Color online) Coefficient of restitution measurements on PMMA: comparison before (a) and after (b) cleaning the balls with acetone and isopropyl alcohol.

i^{th} collision $v_f^i = g t_{air}^i/2 = v_0^{i+1}$. The total time the ball spends in the air between the ith and $i+1^{th}$ collisions $t_{air}^i = t_p^{i+1} - t_p^i - t_c^i$. In these equations, t_p^i is the arrival time of the direct P-wave radiated from the ith collision, t_c^i is the contact time of the same collision, and g is acceleration due to gravity. Drag forces due to air resistance, estimated using a simple model of a sphere in a fluid (Schlichting, 1979), were also incorporated into the calculation of incoming and rebound velocities for the data presented in Figs. 9 and 10. Errors in *e* estimates associated with air resistance are expected to be negligible for low velocities and could increase to about 1% for smaller, less massive balls at higher velocities. For these figures, data is grouped into logarithmically spaced bins on a velocity scale. Each symbol location denotes the median *e* from sets of at least four data points, and the vertical error bar extends from the first to the third quartiles of the data set. Note that the scale in Figs. 9(a) and 9(b) is different from that in Figs. 9(c) and 9(d).

The *e* results reported here are consistent with that of Tillet (1954) for PMMA at room temp, but since all experiments in this study were performed at the same temperature, effects of viscoelasticity were not apparent.

V. DISCUSSION

A. Momentum and energy

The comparison between the force pulse and *e* highlights the fundamental distinction between momentum and energy, and how each relates to radiated stress waves. The force pulse describes the ball's change in momentum, which is conserved, while *e* relates to the efficiency of kinetic energy transfer. In general, even when *e* results indicated that a large amount of the ball's kinetic energy was consumed during the collision, the stress wave signature remained largely unaffected. Figure 7 shows the direct proportionality between the ball's change in momentum and stress waves, even for low *e* collisions. Kinetic energy lost to anelastic processes—and radiated stress waves themselves—during the collision will result in a small reduction in the ball's change in momentum, and therefore, a small reduction in the amplitude of the radiated stress waves, but the (currently measurable) frequency content of the waves will remain largely unchanged. For the case of the "low restitution drop" shown in Fig. 7(b) inset and Fig. 8, over half of the ball's kinetic energy was absorbed during the collision, yet the resulting stress wave signature is not drastically different from that of the Hertz-derived theory, which does not account for any energy loss at all. The only clues in the stress wave signature which indicate that an inelastic collision has taken place are the subtle changes in the ball's momentum transfer such as the small precursory force, slight asymmetry, and approximately 20% reduction in amplitude of the force pulse. (These subtle changes are discussed in greater detail in Sec. V C.) This conclusion emphasizes the difficulties of studying energy-related seismic-source phenomena via radiated stress waves, and reinforces the ball impact as reliable source of stress waves despite energy-related deviations from Hertzian theory.

For collisions at moderate velocities ($v_0 \sim 1$ m/s), the force pulse was adequately modeled by Hertzian theory even when permanent plastic deformation was observed. This observation is consistent with those of Tillet (1954) and Lifshitz and Kolsky (1964), who showed that the duration of contact, t_c, does not deviate appreciably from that predicted by Hertzian theory even for incoming velocities eight times greater than that at which plastic deformation is expected to commence (Davies, 1949). The location of zeros found in the spectral content of recorded stress waves shown in Fig. 5 are very close to $f_{zero,n} = n + 0.75$ which clearly supports the "$\sin^{3/2}$" force pulse of Eq. (5) over the "half sine" pulse of Eq. (3) (which would produce $f_{zero,n} = n + 0.5$). Though departures from Hertzian theory such as plastic deformation and surface effects produced some observable changes in the stress wave signature (discussed below), these deviations were slight.

B. Plastic deformation

Plastic deformation was observed for collisions on the steel and aluminum plates, characterized by a sharp decrease in *e* with increasing v_0, shown in Figs. 9(a) and 9(b). More subtle indications of gross yielding include (1) a slight asymmetry and lower-than-expected amplitude of the force pulse, (2) tiny (~ 100 μm) dents left in the plate material, and (3) minor spectral changes in radiated stress waves such as a reduction in $f_{zero,1}$ and an increase in $f_{zero,2}$ and $f_{zero,3}$. The collisions of glass balls on the steel plate were considerably more elastic than those of ruby and steel balls on the steel plate. This result was expected from Hertz theory because the glass balls are less massive (which causes the maximum impact force to be lower) and more compliant (which causes the force to be distributed over a larger contact area). The spectral properties of the collisions of the 2.5 mm glass balls on the aluminum plate were inconsistent with previously mentioned trends; the authors cannot account for this divergence from theory.

For the collisions of all the balls on the glass and PMMA plates, measured e values were much closer to Hertzian-derived predictions by Hunter (1957) and Reed (1985), and the subtle indications of gross plastic deformation described in the previous paragraph were absent. Even though the yield stress of PMMA is lower than that of steel and aluminum, the compliance of this plate material produces a larger area of contact and a longer contact duration, which reduces the maximum stresses developed during the collision.

Counter to the prediction by Hutchings (1979), even when a significant amount of plastic deformation occurred during a collision (as evidence by $e \sim 0.7$), the asymmetry of the force pulse was found to be minor. The lack of asymmetry of the force pulse and its general insensitivity to plastic yielding are likely due to strain rate effects. Also mentioned in Hutchings (1977) and Goldsmith and Lyman (1960), the rate of loading and unloading during the collision of a small ball on a massive body is so great that there simply isn't enough time for plastic deformation to fully develop, and stresses in excess of the yield stress may exist for a short period of time. The loading rate is faster for smaller balls than larger ones, and this is thought to be the reason why higher e was measured for the small balls than the large ones for collisions between steel and ruby balls on the steel plate, as shown in Fig. 9(a).

C. Surface effect

Surface properties such as roughness (Lifshitz and Kolsky, 1964) and adhesion (e.g., Johnson and Greenwood, 1997) were previously suggested as a likely cause for energy loss during impact. In the current study, a "surface effect" was manifested as a decreased average value, and increase in scatter, in e measurements at very low v_0. This was observed for all ball and plate material combinations. Particularly low e collisions were accompanied by a tiny precursory force preceding the main force pulse. A very prominent example of this is shown in Fig. 8. The duration and strength of this curious precursory force was well correlated with the decrease in e. From the duration of the precursory force and the incoming velocity of the ball, the spatial extent of the surface irregularity required to make the force was estimated to be 1 to 4 μm for the largest precursory forces observed. These estimates were consistent with observations of small particles on the surface of the balls when viewed under a microscope. As shown in Fig. 10, surface effects were diminished when the balls were cleaned with acetone and isopropyl alcohol and dropped with a fine sponge instead of from the fingers. Despite this reduction, surface effects are a likely cause for the departure from theory (Reed, 1985) for low v_0 collisions shown in Fig. 10(b). Note that all data shown in Fig. 9 are the result of "after cleaning" experimental conditions.

The observed surface effects suggest that as the two colliding bodies first begin to interact, before full mechanical contact has been formed in the Hertzian sense, the real area of contact is small compared to the size of surface imperfections. At this stage, any roughness or surface imperfections such as grease or dust which may exist between the two surfaces are loaded and deformed, and this deformation saps some small amount of the ball's kinetic energy. For bodies with an abundance of kinetic energy and small contact areas, surface effects can be ignored, but for micro particles impacting real, unclean surfaces, these effects can be significant.

VI. CONCLUSIONS

Recordings of radiated stress waves contain information about the source, propagation medium, and sensor. A set of experiments using multiple sources (ball and capillary), sensors, source-sensor orientations, and test blocks were designed so that the contributions from each of these factors could be systematically identified. The results of this study demonstrate that the impact of a small (1 to 2.5 mm diameter) ball on a suitably massive body is a repeatable and reliable source of stress waves in solid materials, even when moderate yielding of the plate material is observed. For collisions at moderate velocities (~ 1 m/s), the stress wave signature can be adequately modeled by a "$\sin^{3/2}$" force pulse derived from Hertz contact theory [Eq. (5)]. While capillary fracture is an ideal source of high frequency stress waves, a ball impact can serve as an effective complement due to its repeatability, predictability, and the ease at which the frequency content and amplitude of the introduced waves can be modified simply by changing the incoming velocity, size and material of the impinging ball.

Radiated stress waves were found to be linearly proportional to the change of the ball's momentum, even when simultaneous measurements of the ball's coefficient of restitution (e) indicated that a large amount of the ball's initial kinetic energy was consumed by non-conservative processes such as plastic deformation of the plate material. This result suggests that the impulse rather than the energy of radiated stress waves is the physical quantity which best describes strength of the source. This has long been known in seismology where the strength of an earthquake is judged by its seismic moment; energy remains an elusive parameter.

This study emphasizes that stress wave recordings could not be used to measure kinetic energy consumption directly. Instead, phenomena such as plasticity and surface effects were only identified by subtle changes in the calculated force pulse. Plastic yielding in the steel and aluminum plates was marked by a very slight asymmetry of the force pulse and slight changes in the spectral content of radiated stress waves, but these effects were minor, likely muted by strain rate effects. Plastic yielding may play a more important role during the collision of a larger ball with a longer duration of contact.

Variability in the coefficient of restitution was found to be a function of surface cleanliness; force-time pulses recorded from collisions with an abnormally low e were marked by a tiny precursory force indicative of μm scale structures (dust) or roughness on the surfaces which are loaded and inelastically deformed.

The shape of the frequency response $I_{norm}(\omega)$ of the conical piezoelectric sensors used in this study was found to

be unchanged (to within ±3 dB) when coupled to the four different plate materials, with the differences easily removed by deconvolution due to the smoothness of its amplitude and phase spectra (there were no apparent poles or zeros). Consequently, measurements of high frequency surface displacements down to a few pm in amplitude could be attained. The absolute sensitivity, β, of the sensors was found to be highly variable and dependent on the mechanical bond between the sensor tip and specimen, which emphasizes the need for a repeatable calibration source such as ball impact which delivers waves of a known amplitude and frequency content into a solid body.

ACKNOWLEDGMENTS

The authors gratefully acknowledge Professor Lane Johnson for many helpful discussions. This work was funded by NSF-GRF and NSF Grant No. CMS-0624985.

Aki, K., and Richards, P. G. (**1980**). *Quantitative Seismology: Theory and Methods* (Freeman, San Francisco), Chap. 2, pp. 9–36.

Bernstein, A. (**1977**). "Listening to the coefficient of restitution," Am. J. Phys. **45**, 41–44.

Boltz, E. S., and Fortunko, C. M. (**1995**). "Absolute sensitivity limits of various ultrasonic transducers," in Proceedings of the IEEE Ultrasonics Symposium, New York, edited by B. R. McAvoy, pp. 951–954.

Breckenridge, F., and Greenspan, M. (**1981**). "Surface-wave displacement: Absolute measurements using a capacitive transducer," J. Acoust. Soc. Am. **69**, 1177–1185.

Breckenridge, F., Proctor, T., Hsu, N., Fick, S., and Eitzen, D. (**1990**). "Transient sources for acoustic emission work," in *Progress in Acoustic Emission V*, edited by K. Yamaguchi, H. Takahashi, and H. Niitsuma, (The Japanese Society for NDI, Sendai, Japan), pp. 20–37.

Breckenridge, F., Tscheigg, C., and Greenspan, M. (**1975**). "Acoustic emission: Some applications of Lamb's problem," J. Acoust. Soc. Am. **57**, 626–631.

Buttle, D. J., and Scruby, C. B. (**1990**). "Characterization of particle impact by quantitative acoustic emission," Wear **137**, 63–90.

Ceranoglu, A., and Pao, Y. (**1981**). "Propagation of elastic pulses and acoustic emission in a plate," Trans. ASME, J. Appl. Mech. **48**, 125–147.

Chang, C., and Sun, C. T. (**1989**). "Determining transverse impact force on a composite laminate by signal deconvolution," Exp. Mech. **29**, 414–419.

Ching, J., To, A., and Glaser, S. (**2004**). "Microseismic source deconvolution: Wiener filter versus minimax, fourier versus wavelets, and linear versus nonlinear," J. Acoust. Soc. Am. **115**, 3048–3058.

Crook, A. W. (**1952**). "A study of some impacts between metal bodies by a piezoelectric method," Proc. R. Soc. London, Ser. A **212**, 377–390.

Davies, R. M. (**1949**). "The determination of static and dynamic yield stresses using a steel ball," Proc. R. Soc. London, Ser. A **197**, 416–432.

Falcon, E., Laroche, C., Fauve, S., and Coste, C. (**1998**). "Behavior of one inelastic ball bouncing repeatedly off the ground," Eur. Phys. J. B **3**, 45–57.

Glaser, S., Weiss, G., and Johnson, L. (**1998**). "Body waves recorded inside an elastic half-space by an embedded, wideband velocity sensor," J. Acoust. Soc. Am. **104**, 1404–1412.

Goldsmith, W. (**2001**). *Impact* (Dover, New York), Chap. IV, pp. 82–90.

Goldsmith, W., and Lyman, P. T. (**1960**). "The penetration of hard-steel spheres into plane metal surfaces," Trans. ASME, J. Appl. Mech. **27**, 717–725.

Graff, K. (**1975**). *Wave Motion in Elastic Solids* (Oxford University Press, Mineola, NY), Chap. 5, pp. 273–310.

Greenspan, M. (**1987**). "The NBS conical transducer: Analysis," J. Acoust. Soc. Am. **81**, 173–183.

Hertz, H. (**1882**). "Über die Berührung fester elastischer Körper (On the vibration of solid elastic bodies)," J. Reine Angew. Math. **92**, 156–171.

Hsu, N. (**1977**). U.S. Patent No. 4,018,084.

Hsu, N. (**1985**). "Dynamic Green's functions of an infinite plate—A computer program," Technical Report No. NBSIR 85–3234, National Bureau of Standards, Center for Manufacturing Engineering, Gaithersburg, MD.

Hsu, N., and Breckenridge, F. (**1981**). "Characterization of acoustic emission sensors," Mater. Eval. **39**, 60–68.

Hunter, S. C. (**1957**). "Energy absorbed by elastic waves during impact," J. Mech. Phys. Solids **5**, 162–171.

Hutchings, I. M. (**1977**). "Strain rate effects in microparticle impact," J. Phys. D: Appl. Phys. **10**, L179–L184.

Hutchings, I. M. (**1979**). "Energy absorbed by elastic waves during plastic impact," J. Phys. D: Appl. Phys. **12**, 1819–1824.

Johnson, K. (**1985**). *Contact Mechanics* (Cambridge University Press, Cambridge), pp. 351–369.

Johnson, K., and Greenwood, J. (**1997**). "An adhesion map for the contact of elastic spheres," J. Colloid Interface Sci. **192**, 326–333.

Knopoff, L. (**1958**). "Surface motions of a thick plate," J. Appl. Phys. **29**, 661–670.

Lange, Y., and Ustinov, E. (**1983**). "Acoustic pulses excited by impacts on objects—Their analytical representation and spectra," Sov. J. Nondestruct. Test. **105**, 825–830.

Lifshitz, J. M., and Kolsky, H. (**1964**). "Some experiments on anelastic rebound," J. Mech. Phys. Solids **12**, 35–43.

Love, A. E. H. (**1927**). *A Treatise on the Mathematical Theory of Elasticity* (Cambridge Univeristy Press, London), Chap. 8, pp. 184–203.

McLaskey, G., and Glaser, S. (**2009**). "High-fidelity conical piezoelectric transducers and finite element models utilized to quantify elastic waves generated from ball collisions," in Proceedings of the SPIE, Sensors and Smart Structures Technologies for Civil, Mechanical, and Aerospace Systems, edited by M. Tomizuka, C. Yun, and V. Giurgiutiu, Vol. **7292**, pp. 72920S-1–72920S-18.

Michaels, J. (**1982**). "Fundamentals of deconvolution with applications to ultrasonics and acoustic emission," MS thesis, Cornell University, Ithaca, NY.

Michaels, J., Michaels, T. E., and Sachse, W. (**1981**). "Applications of deconvolution to acoustic emission signal analysis," Mater. Eval. **39**, 1032–1036.

Miller, R. K., and McIntire, P. (**1987**). *Nondestructive Testing Handbook Second Edition Vol. 5: Acoustic Emission Testing* (American Society for Nondestructive Testing, Columbus, OH), pp. 121–134.

Pekeris, C. L. (**1955**). "The seismic surface pulse," Proc. Natl. Acad. Sci. U.S.A. **41**, 469–480.

Proctor, T. M. (**1982**). "An improved piezoelectric acoustic emission transducer," J. Acoust. Soc. Am. **71**, 1163–1168.

Reed, J. (**1985**). "Energy losses due to elastic wave propagation during an elastic impact," J. Phys. D **18**, 2329–2337.

Sansalone, M. J., and Street, W. B. (**1997**). *Impact Echo: Nondestructive Evaluation of Concrete and Masonry* (Bulbrier Press, Ithaca, NY), Chap. 3, pp. 29–46.

Schlichting, H. (**1979**). *Boundary-Layer Theory*, 7th ed. (McGraw-Hill, New York), Chap. 1, pp. 5–23.

Scruby, C., and Drain, L. (**1990**). *Laser Ultrasonics: Techniques and Applications* (Taylor & Francis, London), pp. 1–324.

Scruby, C., Stacey, K., and Baldwin, K. G. (**1986**). "Defect characterization in three dimensions by acoustic emission," J. Phys. D: Appl. Phys. **19**, 1597–1612.

Stump, B., and Johnson, L. (**1977**). "The determination of source properties by the linear inversion of seismograms," Bull. Seismol. Soc. Am. **67**, 1489–1502.

Tillet, J. P. A. (**1954**). "A study of the impact of spheres on plates," Proc. R. Soc. London, Ser. B **69**, 677–688.

To, A., and Glaser, S. (**2005**). "Full waveform inversion of a 3-D source inside an artificial rock," J. Sound Vib. **285**, 835–857.

Yilmaz, O. (**1987**). *Seismic Data Processing* (Society of Exploration Geophysicists, Tulsa, OK), Chap. 2, pp. 82–153.

Zener, C. (**1941**). "The intrinsic inelasticity of large plates," Phys. Rev. Lett. **59**, 669–673.